AIR-SIDE PERFORMANCE OF A MICRO-CHANNEL HEAT EXCHANGER IN WET SURFACE CONDITIONS

by

Raviwat SRISOMBA[a], Lazarus Godson ASIRVATHAM[b], Omid MAHIAN[c], Ahmet Selim DALKILIC[d] Mohamed M. AWAD[e], and Somchai WONGWISES[a*]

[a] Fluid Mechanics, Thermal Engineering and Multiphase Flow Research Laboratory, Department of Mechanical Engineering, Faculty of Engineering, King Mongkut's University of Technology Thonburi, Bangkok, Thailand
[b] Department of Mechanical Engineering, Karunya University, Coimbatore, Tamil Nadu, India
[c] Renewable Energies, Magnetism and Nanotechnology Laboratory, Department of Physics, Faculty of Science, Ferdowsi University of Mashhad, Mashhad, Iran
[d] Heat and Thermodynamics Division, Department of Mechanical Engineering, Faculty of Mechanical Engineering, Yildiz Technical University, Yildiz, Istanbul, Turkey
[e] Department of Mechanical Power Engineering, Mansoura University, Mansoura, Egypt

Original scientific paper
DOI:10.2298/TSCI150906227S

The effects of operating conditions on the air-side heat transfer, and pressure drop of a micro-channel heat exchanger under wet surface conditions were studied experimentally. The test section was an aluminum micro-channel heat exchanger, consisting of a multi-louvered fin and multi-port mini-channels. Experiments were conducted to study the effects of inlet relative humidity, air frontal velocity, air inlet temperature, and refrigerant temperature on air-side performance. The experimental data were analyzed using the mean enthalpy difference method. The test run was performed at relative air humidity's ranging between 45% and 80%; air inlet temperature ranges of 27, 30, and 33 °C, refrigerant-saturated temperatures ranging from 18 to 22 °C, and Reynolds numbers between 128 and 166. The results show that the inlet relative humidity, air inlet temperature, and the refrigerant temperature had significant effects on heat transfer performance and air-side pressure drop. The heat transfer coefficient and pressure drop for the micro-channel heat exchanger under wet surface conditions are proposed in terms of the Colburn factor and Fanning factor.

Key words: *automotive air-conditioning, heat transfer coefficient, micro-channel heat exchanger, pressure drop, R-134a*

Introduction

Micro-channel heat exchangers are widely used in many air-conditioning system applications (*e. g.*, automotive air conditioning, mobile air conditioning, and heat pump systems). Because of their specific structure, compactness, light weight, minimal refrigerant usage, and higher heat transfer performance compared to conventional fin-and-tube heat exchangers, micro-channel heat exchangers are a potential alternative for air-conditioning in the future.

* Corresponding author, e-mail: somchai.won@kmutt.ac.th

Many investigations have studied the effects of fin geometries on the air-side performance of louvered fin-and-flat tube heat exchangers under dry and wet surface conditions [1-6]. McLaughlin and Webb [1] investigated the effects of louver pitch and fin pitch under wet surface conditions. Their results showed that air-side pressure drop was larger for a small fin pitch than a large fin pitch due to the increasing condensate retention between the louvered fins. Kim and Bullard [2] presented an experimental study on air-side heat transfer and pressure drop in dry surface conditions. They concluded that the heat transfer coefficient decreased when the flow depth increased, and increased when the air velocity increased. Air-side pressure drop increased as the louvered angle increased and decreased as fin pitch increased. Kim and Bullard [3] remarked that larger fin pitches and louvered angle improved the heat transfer coefficient in wet conditions, especially through high Reynolds numbers.

Kim and Cho [4] experimentally studied the effect of fin pitch and louver angle on air-side performance. They found that the louver angles had little effect on the heat transfer coefficient at fin pitch 1.4 mm. Qi *et al.* [5] compared the differences of fin geometries in mini-channel evaporators by using R-22 as the working fluid in the system. They found that the cooling capacity for a corrugated louvered fin evaporator was better than that of the flat louvered fin evaporator. Cho and Cho [6] experimentally studied the effect of refrigerant mass flow rate, inlet vapor quality and the inclination angle of the test section on the cooling capacity. They found that the cooling capacity increased with increasing refrigerant mass flow rate and inclination angle (from vertical). On the other hand, the cooling capacity decreased with increasing the vapor quality. Kim *et al.* [7, 8] studied the effects of inclination angle and relative humidity on heat transfer and pressure drop for a micro-channel heat exchanger in both dry and wet conditions. They found that the inclination angle ($-60^{o} < \theta < 60^{o}$) had no significant effect on the heat transfer coefficient, while the pressure drop also increased as the inclination angle increased. Also, they found that relative humidity had no effect on heat transfer and pressure drop for the larger fin pitches. Recent studies have focused on the effects of fin geometry, test operating, surface coating, and frosting phenomena on the fin and tube of the micro-channel heat exchanger, which is important to the development of heat pump systems [9-12].

Although there are a number of papers on the air-side performance of a micro-channel heat exchanger, most of these studies have used water as a working fluid in tube side. Despite its importance in the refrigerating applications, no attention was paid to the air-side performance of a micro-channel heat exchanger working with refrigerants. Up to now, there have been only three works, carried out by [5, 6, 11], dealing with the refrigerants. However, the experimental apparatus used in these three studies could not provide a wide range of the experimental conditions for both air side and tube side. The heat transfer coefficient and pressure drop which are very important indicators in the thermal performance of the heat exchanger have also not been mentioned. As a consequence, in the present study, the main concern is to study the heat transfer performance and frictional characteristics of micro-channel heat exchangers in wet surface conditions working with R-134a. A closed loop wind tunnel equipped with complete instruments, obtained from special design and construction was used in the present study. The effects of air inlet relative humidity, air inlet temperature, air velocity, and refrigerant-saturated temperature on the air-side performance of the heat exchanger under wet surface conditions, which have not yet appeared in open literature, are presented.

Experimental apparatus and procedure

The schematic diagram for the experimental micro-channel heat exchanger apparatus is presented in fig. 1. The main components of the system include a test section, refrigerant loop, cooling water loop, air tunnel loop, quick-closing valve system, and a data acquisition system.

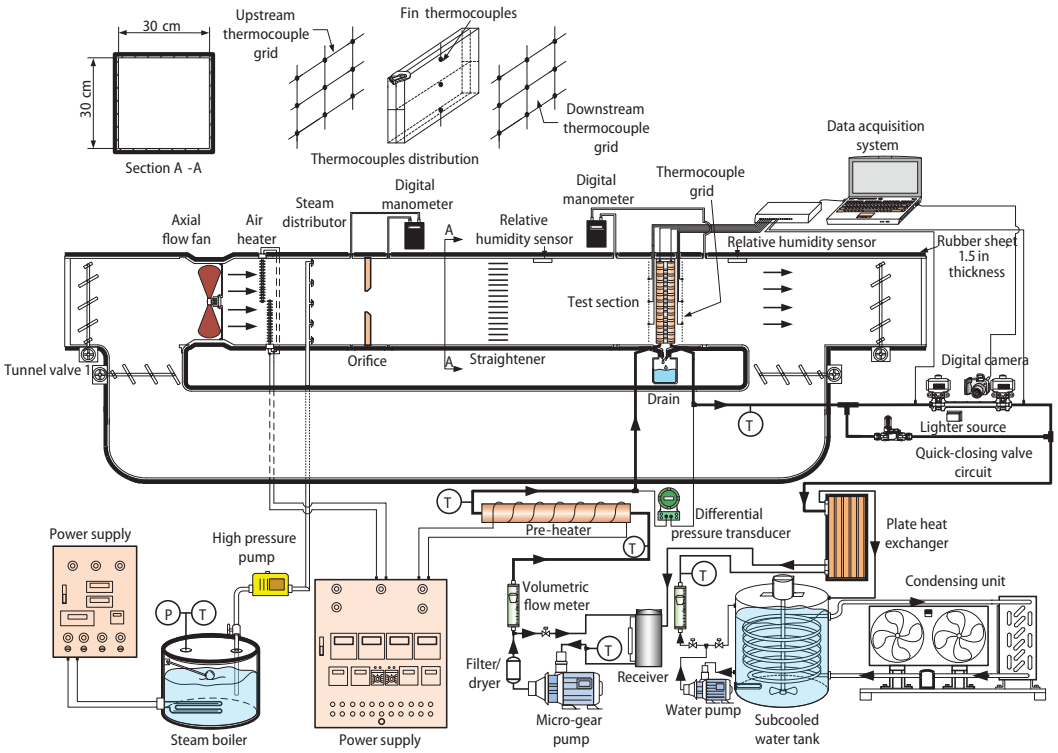


Figure 1. Schematic diagram of experimental apparatus

Refrigerant loop

In the refrigerant loop, liquid refrigerant is pumped by a gear pump, which can be regulated with an inverter. The refrigerant then flows through a filter/dryer, a refrigerant flow meter, pre-heater, and a sight glass tube, and then into the test section. The vapor quality before entering the test section can be calculated by the heat balance of the pre-heater. A DC power supply is used to apply the imposed heat flux to the pre-heater, which can be controlled by adjusting the supply voltage and current. After leaving the test section, the outlet vapor quality of the refrigerant can be estimated by the correlation with the void fraction. The refrigerant vapor then condenses in a plate heat exchanger of the cooling water loop and is later collected in a receiver tank. It eventually returns to the micro-gear pump to complete the cycle.

Air tunnel loop

Figure 1 also shows the schematic diagram of the air tunnel loop. The air tunnel is designed for both closed-and opened-loop operating conditions. The rectangular air duct is made from a galvanized steel sheet measuring 300 mm × 300 mm. The duct walls are thermally insulated with 1.5-inch-thick rubber sheet insulation (Aeroflex Products). The volume flow rate of air is measured with an orifice meter based on the ISO 5167-1 (1991) [13]. The pressure drops across the orifice meter and the test section are measured by using a digital manometer with an accuracy of ±0.5%. The air is circulated with an axial flow fan and flows through the heating section, humidification sections, and test section of the main tunnel. The air inlet temperature and humidity are controlled before entering test section. The upstream and

Table 1. Uncertainties of measured quantities and calculated parameters

Parameter	Uncertainty
Temperature	±0.1 °C
Mass flow rate of refrigerant	±0.1 of full scale
Reynolds number, Re_{Lp}	±0.11 %
Vapor quality inlet, x_{in}	±4.85 %
Vapor quality outlet, x_{out}	±1.21 %
Heat transfer coefficient, h_o	±0.33 %
Colburn j factor	±1.17 %
Friction f factor	±3.80 %

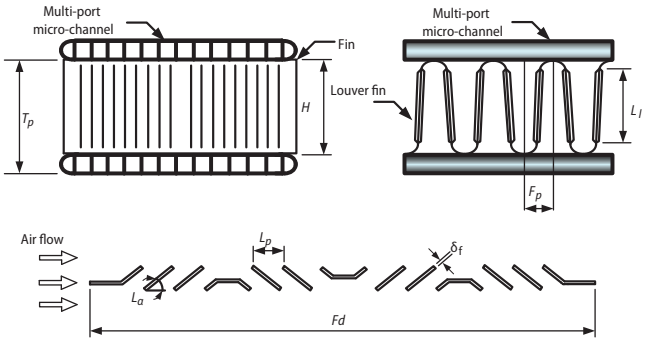


Figure 2. Schematic diagram of the test section

Table 2. Configurations of the micro-channel heat exchanger

	Item	Specification
Tube	Tube depth per slab [mm]	19
	Tube length [mm]	243
	Tube and wall thickness, δ_{wall} [mm]	0.25
	Tube pitch, T_p [mm]	6.65
	Hydraulic diameter [mm]	1.10
	Number of channel	14
Fin	Fin height, H [mm]	4.85
	Fin pitch, F_p [mm]	1.3
	Flow depth, F_d [mm]	19
	Fin thickness, δ_f [mm]	0.1
	Louver angle, L_a [°]	32
	Louver pitch, L_p [mm]	0.9
	Louver length, L_l [mm]	4.2

downstream temperatures of the air across the test section are measured by the thermocouple grids, which are installed at the front and back sides of the tested section. Each grid consists of nine T-type thermocouples. Each thermocouple grid has three columns and three rows, their arrangement is also shown in fig. 1. All of the signals from the thermocouples, both at the air-side and refrigerant-side, were recorded by a data acquisition system. The maximum uncertainties of the measured quantities and calculated parameters are shown in tab. 1.

Test section

In this study, the test section is an aluminum micro-channel heat exchanger, which consists of the multi-louvered fins and multi-port mini-channels. The details of the fin and tube geometries and the parameters of the test section are presented in fig. 2. The details of the test section's configurations and the test conditions are presented in tabs. 2 and 3, respectively.

Data reduction

The heat transfer rate required to calculate the air-side heat transfer coefficient is the average of Q_a and Q_r, namely:

$$Q_{avg} = \frac{Q_a + Q_r}{2} \tag{1}$$

where Q_a and Q_r are the air-side heat transfer rate and refrigerant-side heat transfer rate, respectively, as defined by:

$$Q_a = \dot{m}_a \left[(i_{a,in} - i_{a,out}) + (W_{a,in} - W_{a,out}) i_{fw} \right] \tag{2}$$

$$Q_r = \dot{m}_r (i_{r,out} - i_{r,in}) \tag{3}$$

where $\dot{m}_r$ is the refrigerant mass flow rate and $i_{r,out}$ and $i_{r,in}$ are the outlet enthalpy and inlet enthalpy of the refrigerant, respectively. The rate of the water condensation can be determined by:

$$\dot{m}_{cond} = \dot{m}_a (W_{a,in} - W_{a,out}) \tag{4}$$

The inlet and outlet enthalpy of refrigerant-side can be determined:

$$i_{r,\text{in}} = \frac{IV}{\dot{m}_\text{r}} - i_{f,T_{pre}} \tag{5}$$

$$i_{r,\text{out}} = i_{f,Tts} - x_\text{out} i_{fg,Tts} \tag{6}$$

where x_out can be calculated by iteration from the void fraction correlation for annular flow regime, as proposed by Srisomba *et al.* [14]:

Table 3. Experimental conditions

Air-side conditions	
Air inlet temperature [°C]	27-33
Air inlet relative humidity [%]	45-80
Air frontal velocity [ms^{-1}]	1.7-2.1
Refrigerant-side conditions	
Refrigerant saturated temperature [°C]	18-22

$$\alpha_\text{ann} = \left[1 + 4.331\left(\frac{1-x}{x}\right)^{1.073}\left(\frac{\rho_v}{\rho_l}\right)^{1.041}\left(\frac{\mu_l}{\mu_v}\right)^{0.008}\right]^{-1} \tag{7}$$

The overall heat transfer coefficient $U_o A_o$ is based on the enthalpy potential and is given:

$$Q_\text{avg} = U_\text{o} A_\text{o} \Delta i_m \tag{8}$$

where Δi_m is the logarithmic mean enthalpy difference for the counter flow coil:

$$\Delta i_m = \frac{(i_{a,\text{in}} - i_{s,r,\text{out}}) - (i_{a,\text{out}} - i_{s,r,\text{in}})}{\ln\dfrac{\left(i_{a,\text{in}} - i_{s,r,\text{out}}\right)}{\left(i_{a,\text{out}} - i_{s,r,\text{in}}\right)}} \tag{9}$$

The overall thermal resistance is:

$$\frac{1}{U_\text{o} A_\text{o}} = \frac{b_r^{'}}{h_\text{i} A_\text{i}} + \frac{b_t^{'}\delta_\text{wall}}{k_t A_{t,\text{m}}} + \frac{b_w^{'}}{h_{\text{o,w}} A_{\text{o,w}} \eta_{\text{o},w}} \tag{10}$$

where $h_{\text{o,w}}$ is the heat transfer coefficient for a wet surface. This can be estimated by:

$$h_{\text{o,w}} = \frac{1}{\left(\dfrac{c_{p,a}}{b_{w,f}^{'} h_\text{o}} + \dfrac{y_w}{k_w}\right)} \tag{11}$$

where y_w is the thickness of the water film and it is a constant of 0.127 mm (0.005 inches) [15], and k_w is the thermal conductivity. The surface effectiveness and fin efficiency for a wet surface can be expressed:

$$\eta_{\text{o,w}} = 1 - \frac{A_f}{A_o}\left(1 - \eta_{f,w}\right) \tag{12}$$

$$\eta_{f,w} = \frac{\tanh(ml)}{ml} \tag{13}$$

$$m = \sqrt{\frac{2h_\text{o}}{k_f \delta_f}\frac{b_w}{c_{p,a}}\left(1 + \frac{\delta_f}{F_d}\right)} \tag{14}$$

$$l = \frac{H}{2} - \delta_t \tag{15}$$

The refrigerant side heat transfer coefficient h_i is evaluated according to Kaew-On and Wongwises [16]:

$$h_i = SBo^{1.032} We_l^{0.052} Co^{-0.391} h_{sp} \tag{16}$$

The quantities of b_r' and b_t' can be calculated:

$$b_r' = \frac{i_{s,t,i,m} - i_{s,r,m}}{T_{t,i,m} - T_{r,m}} \tag{17}$$

$$b_t' = \frac{i_{s,t,o,m} - i_{s,t,i,m}}{T_{t,o,m} - T_{t,i,m}} \tag{18}$$

The values of b_w' are the slopes of the saturated air enthalpy curves, evaluated at the mean water film temperature at the base surface. The h_o is the sensible heat transfer coefficient for wet surfaces. The Colburn j factor is the parameter that characterizes the air-side heat transfer coefficient in a dimensional form, which is expressed:

$$j = \frac{h_o \, \mathrm{Pr}^{2/3}}{\rho_m V_{max} c_{p,a}} \tag{19}$$

The air-side pressure drop can be expressed as friction f factor, namely:

$$f = \frac{A_{min}}{A_{fr}} \frac{\rho_m}{\rho_{in}} \left[\frac{2\rho_{in} \Delta P_a}{\left(\rho_m V_{max}\right)^2} - \left(K_c + 1 - \sigma^2\right) - 2\left(\frac{\rho_{in}}{\rho_{out}} - 1\right) + \left(1 - \sigma^2 - K_e\right) \frac{\rho_{in}}{\rho_{out}} \right] \tag{20}$$

where K_c and K_e are coefficients for pressure loss at the inlet and outlet of the heat exchanger [17, 18].

Results and discussion

Energy balance

The heat transfer rates obtained from the air-side and refrigerant-side are compared in this section, in order to validate the experimental apparatus and the accuracy of the results. As shown in fig. 3, the energy balances between the air and refrigerant sides of the micro-channel heat exchanger have a relative error of less than 10%.

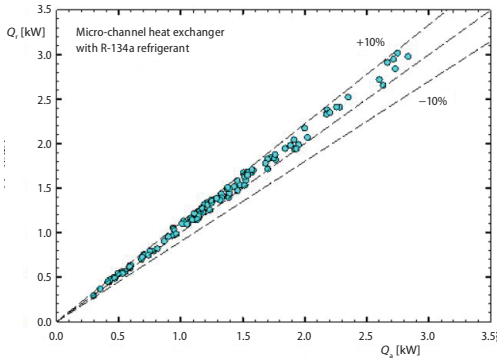


Figure 3. Energy balance between air and refrigerant

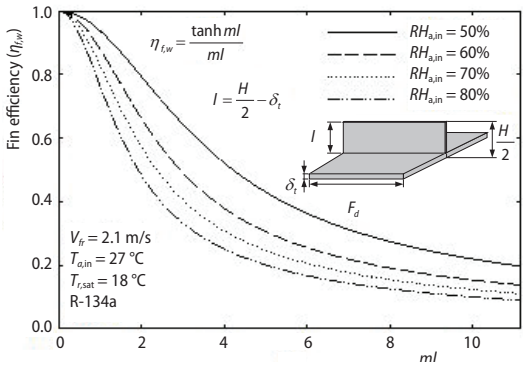


Figure 4. The fin efficiency plotted against *ml*

Wet fin efficiency

The wet fin efficiencies for micro-channel heat exchangers with different relative humidity are presented in fig. 4. As expected, fin efficiency decreases as relative air humidity increases, because increasing the condensation of water vapor on the fin surface leads to increased fin temperature. The ideal rate of heat transfer is higher than the actual rate of heat transfer. Thus, wet fin efficiency is reduced at higher relative humidity.

Average heat transfer rate

The effects of relative humidity, air frontal velocity and air inlet temperature on the average heat transfer rate, Q_{avg}, are presented in figs. 5(a) and 5(b). The data show that the average heat transfers increase as the relative humidity increases. Although the effect of air velocity on the average heat transfer rate is comparatively small, the average heat transfer rates increase slightly as frontal air velocity increases, as shown in fig. 5(a). Figure 5(b) shows that the average heat transfer rates increase as air inlet temperature increases at the same relative humidity.

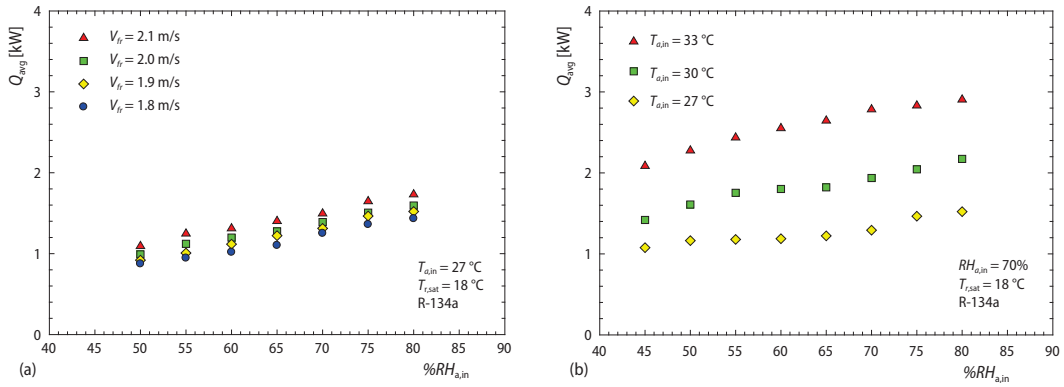


Figure 5. Effect of air frontal velocity; (a) and inlet air temperature, (b) on the heat transfer rate

Heat transfer coefficient

The effects of inlet relative humidity and air inlet temperature on the heat transfer coefficient are presented in figs. 6(a) and 6(b), respectively. The results show that the heat transfer coefficient increases as the inlet relative humidity and air inlet temperature increase at the same air frontal velocity.

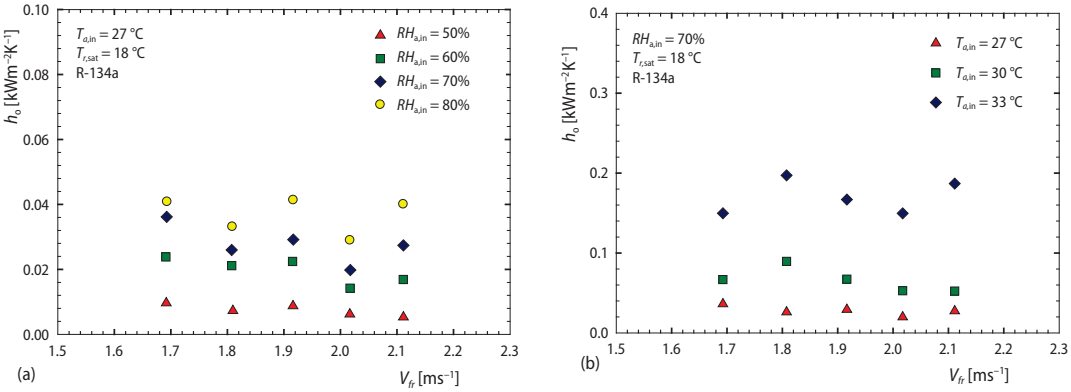


Figure 6. Effect of inlet relative humidity (a) and inlet air temperature (b) on the air-side heat transfer coefficient

This result is analogous to the results from Wang *et al.* [19] and Bourabaa *et al.* [20], who reported that the heat transfer coefficient at higher inlet humidity is larger than at lower inlet humidity. These researchers argued that the presence of droplets on the fin and tube surfaces increase the rough surface and hence result in high heat transfer performance.

Air-side pressure drop

The air-side pressure drops across the micro-channel heat exchanger, with the effects of the frontal air velocity, air inlet temperature and air relative humidity are presented in figs. 7(a) and 7(b), respectively. Figure 7(a) presents variation of the pressure drop with inlet relative humidity for the different air frontal velocities.

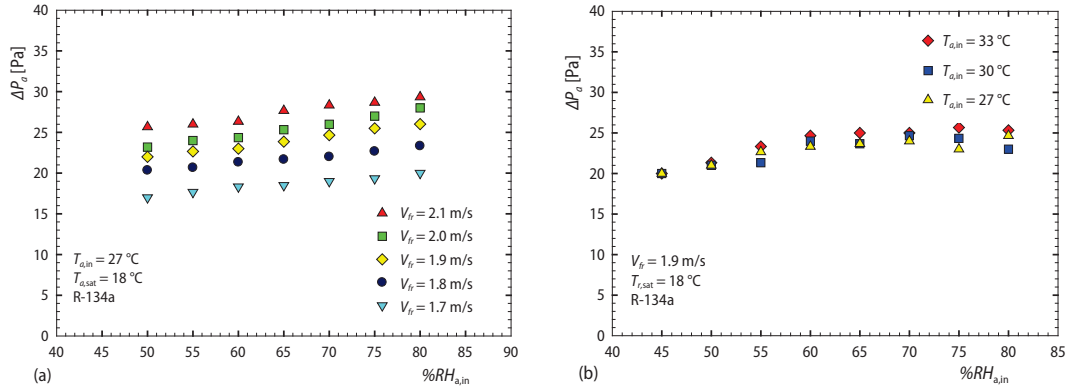


Figure 7. Effect of air frontal velocity (a) and inlet air temperature (b) on the pressure drop

The air-side pressure drops further across the micro-channel heat exchanger as the air frontal velocity increases, as expected. When the air velocity increases, the water droplets on the fin surface can be formed as a water film, which is retained between the louvered fins. Hence, the free flow area for the air is reduced, which leads an increase in the air-side pressure drop. As shown in fig. 7(a), the air-side pressure drop increases slightly as the inlet relative humidity increases.

This result is analogous to that of Boewe *et al.* [21], who found a significant effect of inlet relative humidity on the air-side pressure drop of a micro-channel heat exchanger. However, Kim *et al.* [8] reported that the effect of inlet humidity on a pressure drop is negligible for micro-channel heat exchangers with a larger fin pitch (F_p = 2.1 mm) and louver pitch (L_p = 1.4 mm). This may be due to the different fin geometries. The micro-channel heat exchanger used in this study had a smaller fin pitch (F_p = 1.3 mm) and louver pitch (L_p = 0.9 mm), and the effect of the water retention had a significant effect on the air-side pressure drop.

The effects of the inlet air temperature on the air-side pressure drop at V_{fr} = 1.9 m/s are shown in fig. 8(b). The air temperature had small effects on the air-side pressure drop at the same air frontal velocities.

Colburn factor (j) and friction factor (f)

The Colburn and friction factors obtained from the present study, with the three effects of air frontal velocity, refrigerant-saturated temperature, and inlet relative humidity, are shown in figs. 8(a) and 8(b), respectively.

The results show that the Colburn factors (j) increase as inlet relative humidity and air inlet temperature increase but decrease as refrigerant temperature increases. The friction

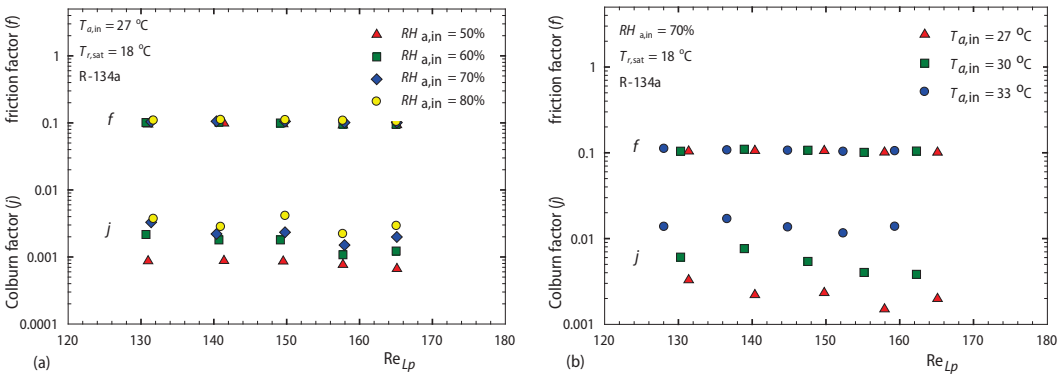


Figure 8. Effect of inlet relative humidity (a) and inlet air temperature (b) on *j* and *f* factors

factors, (*f*), are independent of the variations in Reynolds number, relative humidity, air temperature, and refrigerant temperature.

Conclusions

This study reports the effect of operating conditions on the air-side performance of a micro-channel heat exchanger during the cooling and dehumidification processes. The conclusions can be described as follows.

- The wet fin efficiency rapidly decreases as inlet relative humidity and air inlet temperature increase.
- The dehumidification capacity increases as the air frontal velocity, inlet relative humidity, and air inlet temperature increase, and as the refrigerant's saturated temperature decreases.
- The heat transfer coefficient increases as the inlet relative humidity and air inlet temperature increase, and as the refrigerant's saturated temperature decreases.
- The relative humidity and air frontal velocity have significant effects on the air-side pressure drop for the smaller fin pitch, louver pitch, and flow depth heat exchanger cases, whereas air and refrigerant temperatures have small effects.

Acknowledgement

The first, third, fourth, and sixth authors acknowledge the financial support provided by the "Research Chair Grant" National Science and Technology Development Agency (NSTDA), the Thailand Research Fund (TRF), the National Research University Project (NRU) and King Mongkut's University of Technology Thonburi through the "KMUTT 55th Anniversary Commemorative Fund".

Nomenclature

A_f – surface area of fin, [m^2]
A_{fr} – frontal area, [m^2]
A_i – inside surface area of tube, [m^2]
A_{min} – minimum free flow area for air-side, [m^2]
A_o – total outside surface area, ($= A_{t,o} + A_f$), [m^2]
A_t – tube surface area of tube, [m^2]
Bo – boiling number, ($= q''/G_{lv}$), [-]
b'_r – slope of the air saturation curved at the mean refrigerant temperature and the inside wall temperature, [Jkg^{-1}K^{-1}]
b'_t – slope of the air saturation curved between the outside and the inside wall temperature, [Jkg^{-1}K^{-1}]
b'_w – slope of the air saturation curved at the mean water film temperature and the outside wall temperature, [Jkg^{-1}K^{-1}]
Co – distribution parameter, $\{= [(1-x)/x]^{0.8}(\rho_v/\rho_l)^{0.5}\}$, [-]
$c_{p,a}$ – specific heat, [Jkg^{-1}K^{-1}]
D – tube size diameter, [m]

f – Fanning friction factor, [–]
F_d – flow depth, [m]
F_p – fin pitch, [m]
G – mass flux, [kgm^{-2}s^{-1}]
H – fin height, [m]
h_{sp} – single-phase heat transfer coefficient, [= $0.023\mathrm{Re}_l^{0.8}\mathrm{Pr}_l^{0.4}(k/D)$], [–]
h – heat transfer coefficient, [kWm^{-2}K^{-1}]
I – electric current, [A]
i_a – air enthalpy, [kJkg^{-1}]
i_f – saturated liquid enthalpy of the refrigerant, [kJkg^{-1}]
i_{fg} – difference between saturated vapor enthalpy and saturated liquid enthalpy (= $i_g - i_f$), [kJkg^{-1}]
i_r – refrigerant enthalpy, [kJkg^{-1}]
$i_{s,r,\mathrm{in}}$ – saturated air temperature at the inlet refrigerant temperature, [kJkg^{-1}]
$i_{s,r,\mathrm{out}}$ – saturated air temperature at the outlet refrigerant temperature, [kJkg^{-1}]
$i_{s,r,m}$ – mean saturated air enthalpy at the mean refrigerant temperature, [kJkg^{-1}]
$i_{s,t,i,m}$ – mean saturated air enthalpy at the mean inside tube wall temperature, [kJkg^{-1}]
$i_{s,t,o,m}$ – mean saturated air enthalpy at the mean outside tube wall temperature, [kJkg^{-1}]
Δi_m – log mean enthalpy difference, [–]
j – Colburn j factor, [–]
k_f – thermal conductivity of louver fin, [Wm^{-1}K^{-1}]
k_t – thermal conductivity of tube, [Wm^{-1}K^{-1}]
k_w – thermal conductivity of water film, [Wm^{-1}K^{-1}]
L_l – louver length, [m]
L_p – louver pitch, [m]
L_α – louver angle, [°]
$\dot{m}$ – mass flow rate, [kgs^{-1}]
Pr – Prandtl number, [–]
ΔP_a – air-side pressure drop, [Pa]
Q – heat transfer rate, [kW]
RH – relative humidity, [%]
S – additional factor for two-phase flow heat transfer coefficient, [= $1.737 + 0.97(\beta\phi_l^2)$], [–]
T_a – air temperature, [°C]
T_p – tube pitch, [m]
T_r – refrigerant temperature, [°C]
$T_{t,i,m}$ – mean inside tube surface temperature, [K]
$T_{t,o,m}$ – mean outside tube surface temperature, [K]
U_o – overall heat transfer coefficient, [WK^{-1}m^{-2}]
V – AC voltage, [V]
V_{fr} – air frontal velocity, [ms^{-1}]
$V_{\max}$ – maximum air velocity, [ms^{-1}]
W_a – humidity ratio of moist air, [kgkg^{-1}]
We_l – Webber number, (= $G^2D/\rho\sigma$), [–]
x – vapor quality, [–]
y_w – thickness, [m]

Greek symbols

α – void fraction, [–]
δ_f – fin thickness, [m]
δ_t – tube thickness, [m]
δ_{wall} – tube and wall thickness, [m]
$\eta_{f,w}$ – wet fin efficiency, [–]
$\eta_{o,w}$ – surface effectiveness, [–]
μ_l – liquid dynamic viscosity, [Nsm^{-2}]
μ_v – vapor dynamic viscosity, [Nsm^{-2}]
ρ_{in} – mass density of inlet air, [kgm^{-3}]
ρ_l – liquid mass density of refrigerant, [kgm^{-3}]
ρ_m – mean density of air, [kgm^{-3}]
ρ_{out} – mass density of inlet air, [kgm^{-3}]
ρ_v – vapor mass density of refrigerant, [kgm^{-3}]
σ – surface tension, [Nm^{-1}]

Subscripts

a – air
ann – annular flow regime
avg – average value
cond – condensation
f – fin (louver fin)
i – inside
in – inlet
l – liquid
m – mean value
o – outside
out – outlet
pre – pre-heater
r – refrigerant
sat – saturation
t – tube (multi-port)
ts – test section
v – vapor
w – wet condition

References

[1] Mc Laughlin, W. J., Webb, R. L., Wet Air-Side Performance of Louver Fin Automotive Evaporators, *SAE paper* 2000-01-0574, (2000)
[2] Kim, M.-H., Bullard, C.-W., Air-Side Thermal Hydraulic Performance of Multi-Louvered Fin Aluminum Heat Exchangers, *International Journal of Refrigeration, 25* (2002), 3, pp. 390-400
[3] Kim, M.-H., Bullard, C.-W., Air-Side Performance of Brazed Aluminum Heat Exchangers under Dehumidifying Conditions, *Int. J. Refrigeration, 25* (2002), 7, pp. 924-934
[4] Kim, N.-H., Cho, J.-P., Air-Side Performance of Louver-Finned Flat Aluminum Heat Exchangers at a Low Velocity Region, *Heat Mass Transfer, 44* (2008), 9, pp. 1127-1139

[5] Qi, Z., *et al*., Investigating Performance of New Mini-Channel Evaporators, *Applied Thermal Engineering, 29* (2009), 17-18, pp. 3561-3567
[6] Cho, H., Cho, K., Performance Comparison of Microchannel Evaporators with Refrigerant R-22, *Journal of Mechanical Science and Technology, 22* (2007), Nov., pp. 1926-1934
[7] Kim, M.-H., *et. al.,* Effect of Inclination in the Air-Side Performance of a Brazed Aluminum Heat Exchanger under Dry and Wet Conditions, *Int. J. Heat Mass Transfer, 44* (2001), 24, pp. 4613-4623
[8] Kim, M.-H., *et. al.,* Effect of Inlet Humidity Condition on the Air-Side Performance of an Inclined Brazed Aluminum Evaporator, *Int. J. Refrigeration, 25* (2002), 5, pp. 611-620
[9] Moallem, E., *et. al.,* Experimental Measurements of the Surface Coating and Water Retention Effects on Frosting Performance of Microchannel Heat Exchangers for Heat Pump Systems, *Exp. Therm. Fluid Sci., 39* (2012), May, pp. 176-188
[10] Moallem, E., *et. al.,* Experimental Investigation of Adverse Effect of Frost Formation on Microchannel Evaporators, Part1: Effect of Fin Geometry and Environmental Effects, *Int. J. Refrigerantion, 36* (2013), 6, pp. 1119-1130
[11] Brignoli, R., *et al.,* Experimental Analysis of an Air-Water Heat Pump with Mocro-Channel Heat Exchanger*, Appl. Thermal Eng., 50* (2013), 1, pp. 1119-1130
[12] Xu, B., *et. al.,* Experimental Investigation of Frost and Defrost Performance of Microchannel Heat Exchanger for Heat Pump Systems, *Appl. Energy, 103* (2013), Mar., pp. 180-188
[13] ***, ISO 5167-1, International Standard, Measurement of Fluid Flow by Means of Pressure Differential Devices – Part 1: Orifice Plates, Nozzles and Venturi Tubes Inserted in Circular Cross-Section Conduits Running Full
[14] Srisomba, R., *et al.,* Measurement of the Void Fraction of R-134a Flowing through a Horizontal Tube, *International Communications in Heat and Mass Transfer, 56* (2014), Aug., pp. 8-14
[15] Myers, R. J., The Effect of Dehumidification on the Air-Side Heat Transfer Coefficient for a Finned-Tube Coil, M. Sc. thesis, University of Minnesota, Minneapolis, Minn., USA, 1967
[16] Kaew-On, J., Wongwises, S., New Proposed Two-Phase Multiplier and Evaporation Heat Transfer Coefficient Correlations for R134a Flowing at Low Mass Flux in a Multiport Minichannel, *Int. Commun. Heat Mass Transfer, 39* (2012), 6, pp. 853-860
[17] Kays, W. M., London, A. L., *Compact Heat Exchangers,* 3rd ed., McGraw-Hill Book Company, New York, USA, 1984
[18] Huzayyin, A. S., *et. al.,* Air-Side Performance of a Wavy-Finned-Tube Direct Expansion Cooling and Dehumidifying Air Coil, *Int. J. Refrigeration, 30* (2007), 2, pp. 230-244
[19] Wang, C. C., *et al.,* A Comparison of the Air-Side Performance of the Fin-and-Tube Heat Exchangers in Wet Conditions; with and without Hydrophilic Coating, *Appl. Therm. Eng., 22* (2002), 3, pp. 267-278
[20] Bourabaa, A., *et al.,* The Influence of the Inlet Conditions on the Air Side Heat Transfer Performance of Plain Finned Evaporator, *World Academy of Science, Engineering and Technology, 5* (2011), 11, pp. 20-23
[21] Boewe, D. E., *et al.,* Comparative Experimental Study of Subcritical R134a and Transcriptical R744 Refrigerant Systems for Mobile Applications, ACRC CR-17, University of Illinois at Urbana-Champaign, Campaign, Ill., USA, 1999
[22] Kim, N.-H., Cho, J.-P., Air-Side Performance of Louver-Finned Flat Aluminum Heat Exchangers at a Low Velocity Region, *Heat Mass Transfer, 44* (2008), 9, pp. 1127-1139

Paper submitted: September 6, 2015
Paper revised: September 24, 2016
Paper accepted: September 6, 2016

© 2017 Society of Thermal Engineers of Serbia
Published by the Vinča Institute of Nuclear Sciences, Belgrade, Serbia.
This is an open access article distributed under the CC BY-NC-ND 4.0 terms and conditions